QUANTUM BATTERY SYSTEMS
Analyzing Two-Mode Field Charging, Qubit Interactions, and Environmental Influences

by

Ahmed A. ZAHIA[a], Mahmoud Y. ABD-RABBOU[b,c], Eied Mahmoud KHALIL[d]*, and Saud Al-AWFI[e]

[a] Department of Mathematics, Faculty of Science, Benha University, Benha, Egypt
[b] Mathematics Department, Faculty of Science, Al-Azhar University, Nasr City, Cairo, Egypt
[c] School of Physics, University of Chinese Academy of Science, Beijing, China
[d] Department of Mathematics, College of Science, Taif University, Taiif, Saudi Arabia
[e] Department of Physics, Faculty of Science, Taibah University, Medina, Saudi Arabia

Original scientific paper
https://doi.org/10.2298/TSCI2406179Z

This study investigates the dynamical behaviour of a two-cell (two-atom) quantum battery driven by a two-mode charging field. We explore the influence of varying interaction strengths on the system's performance. This includes increasing the coupling between cells and charging fields, and cells themselves through a dipole interaction and Ising interaction along the z-axis. Additionally, the impact of environmental effects is examined by incorporating decay terms for both the charging fields and the cells. Our analysis focuses on key performance metrics such as stored energy, average power, ergotropy, energy fluctuations, and quantum speed limit time. The results reveal that the environment negatively impacts stored energy, power, and ergotropy, but leads to higher speed limits. Enhanced coupling between the charging fields and the cells improves the studied correlations, promoting efficient energy transfer and decreasing speed limit time. Increasing the coupling between the cells, either via the dipole or Ising interaction, generally exhibits a similar effect. This involves a decrease in maximum achievable energy storage, accompanied by the emergence of more erratic energy fluctuations.

Key words: *quantum battery, two-mode charging field, stored energy, average power, ergotropy, energy fluctuations*

Introduction

In the contemporary era, portable energy storage devices, epitomized by batteries, underpin many applications that permeate our daily lives, these ubiquitous systems power various technologies, from household appliances and medical instrumentation transportation and navigation systems. The efficacy of these devices is intrinsically linked to the efficiency of the underlying energy conversion mechanisms [1-3]. Conventional batteries operate on the principle of electrochemical cells, which facilitate the conversion of chemical energy into electrical energy through redox reactions. However, as the miniaturization of electronic devices continues apace, quantum effects become increasingly influential. This phenomenon presents a captivating opportunity to develop a new generation of devices that surpass their classical counterparts by harnessing the tenets of quantum mechanics [4-8]. A particularly promising avenue in this domain lies in the exploration of quantum batteries (QB). A QB can be defined as an assem-

* Corresponding author, e-mail: eiedkhalil@yahoo.com

blage of one or more quantum systems, typically characterized by two distinct energy levels, that possess the inherent capacity to store energy. The concept of QB garnered significant scientific interest following the pioneering work of Alicki and Fannes in [9].

Theoretically, QB present a paradigm shift in energy storage, harnessing the principles of quantum mechanics to surpass conventional battery technology. Understanding QB performance necessitates delving into two fundamental processes: charging and discharging. Discharging signifies the inevitable energy loss experienced by a QB through interactions with its environment, mirroring a phenomenon observed in classical batteries [10-12]. Conversely, charging entails the utilization of an external energy field to replenish the QB's internal energy reserves [13, 14]. To comprehensively assess the effectiveness of a QB, a multitude of key metrics are employed. These metrics encompass stored energy, ergotropy, charging power, and others [15-17]. The first protocol of QB proposed the potential of entanglement operations to augment the extractable energy from a QB [9]. However, this notion was subsequently contested by Hovhannisyan *et al.* [18] who demonstrated that optimal energy extraction could be achieved through sequential permutation operations, circumventing the need for dynamic entanglement generation. Notably, the implementation of such permutation operations comes at the cost of increased time expenditure. Conversely, collective charging operations that leverage entanglement creation are believed to offer a substantial speedup compared to parallel charging schemes where individual QB cells are charged independently [19]. Disordered interactions within a QB, characterized by the absence of a well-defined order, have been demonstrated to enhance charging power [20]. Additionally, studies have shed light on the influence of disorder and localization on QB behavior. Notably, QB in the many-body localized phase exhibit greater stability and require shorter optimal charging times compared to those in localized phases [21]. The quantum entanglement and coherence, key features of the quantum realm, have also been investigated in the context of two- and three-cell QB [22]. These studies suggest that while entanglement appears to have a minimal or even detrimental effect on efficiency, quantum coherence exhibits a demonstrable correlation with QB performance. However, further research is needed to definitively elucidate the precise role of quantum correlations in QB. While some studies suggest a relationship between QB performance and its correlation content, a clear understanding remains elusive [23]. Recent investigations have explored the impact of using three well-known quantum optical states – Fock, coherent, and squeezed vacuum – as the initial state of the charger [14]. These findings indicate that the coherent state emerges as the optimal choice for both energy deposition and extraction due to its ability to minimize charger-battery entanglement.

Our motivation in this article is to advance the understanding and practical implementation of quantum battery systems through analytical study. This research investigates the energy dynamics, focusing on average charging and discharging power, ergotropy, energy fluctuation, and the quantum speed limit. By solving the quantum battery system analytically, we aim to understand how these metrics are influenced by Hamiltonian parameters, especially interaction parameters, and environmental effects. This study provides a framework for optimizing QB, demonstrating the potential for superior performance and contributing to both theoretical foundations and practical advancements in quantum energy storage.

The model

Let a two-cell QB composed of two-level atoms with identical transition frequencies ω_q. Each cell interacts with a distinct two-mode of a quantized electromagnetic field, characterized by frequencies ω_a and ω_b, respectively. The interaction between the cell system and the charger system is governed by the rotating wave approximation and a coupling strength λ_1.

Furthermore, a dipole-dipole interaction with a coupling constant λ_2 is introduced to account for the interaction between the two cells. Additionally, the Hamiltonian incorporates the effect of an Ising interaction within the cell system, characterized by a coupling exchange constant λ_3. To capture the inevitable energy loss and decoherence experienced by both the atomic and field systems, the model incorporates a term representing these dissipative effects. The physical Hamiltonian of this battery is expressed:

$$\hat{H} = \omega_a \hat{a}^\dagger \hat{a} + \omega_b \hat{b}^\dagger \hat{b} + \frac{\omega_q}{2}\sum_{i=1}^{2}\hat{\sigma}_z^i + \lambda_1 \sum_{i=1}^{2}(\hat{a}^\dagger \hat{b}^\dagger \hat{\sigma}_-^i + \hat{a}\hat{b}\hat{\sigma}_+^i) + \lambda_2(\hat{\sigma}_+^1\hat{\sigma}_-^2 + \hat{\sigma}_-^1\hat{\sigma}_+^2) + \\ + \lambda_3(\hat{\sigma}_z^1\hat{\sigma}_z^2) - i\frac{\gamma}{2}\sum_{i=1}^{2}\hat{\sigma}_+^i\hat{\sigma}_-^i - i\frac{\kappa_a}{2}\hat{a}^\dagger\hat{a} - i\frac{\kappa_b}{2}\hat{b}^\dagger\hat{b} \tag{1}$$

where $\hat{a}^\dagger$ and $\hat{b}^\dagger$ ($\hat{a}$ and $\hat{b}$) correspond to the creation (annihilation) of the two-mode field. The $\hat{\sigma}_+^i$ ($\hat{\sigma}_-^i$) and $\hat{\sigma}_z^i$ (where i can take values 1 or 2) are the standard transition operators for qubits. They adhere to the commutation relations $[\hat{\sigma}_z^i, \hat{\sigma}_\pm^i] = \pm\delta_{(i,j)}\hat{\sigma}_\pm^j$ and $[\hat{\sigma}_+^i, \hat{\sigma}_-^j] = \delta_{(i,j)}\hat{\sigma}_z^j$. The spontaneous emission rate γ of the two-level system and the dissipation of the two mode cavity field into the surrounding environment at a rate κ_a, κ_b. Alternatively, to obtain the temporal wave-vector of this QB, one approach involves assuming a specific initial state for the system. This initial state can be represented:

$$\left|\psi(0)\right\rangle = \left|gg,\alpha,\beta\right\rangle,\ \left|\alpha,\beta\right\rangle = \sum_{n,m=0}^{\infty} z_{nm}\left|n,m\right\rangle,\ z_{nm} = \frac{\alpha^n\beta^m}{\sqrt{n!m!}}e^{\frac{-|\alpha|^2-|\beta|^2}{2}} \tag{2}$$

where $|g\rangle$ is the ground state of the cells, signifying an empty battery, while $|\alpha, \beta\rangle$ represents the coherent state of the two-mode field, functioning as the charger for the system. The temporal wave-vector of the QB is given:

$$\left|\psi(t)\right\rangle = \sum_{n,m=0}^{\infty} A_{nm}(t)\left|ee,n,m\right\rangle + B_{nm}(t)\left|eg,n+1,m+1\right\rangle + C_{nm}(t)\left|ge,n+1,m+1\right\rangle + \\ + D_{nm}(t)\left|gg,n+2,m+2\right\rangle \tag{3}$$

Applying the wave-vector eq. (3) in time-dependant Schrodinger equation:

$$i\frac{\partial}{\partial t}\left|\psi(t)\right\rangle = \hat{H}\left|\psi(t)\right\rangle$$

we can get the following linear ordinary differential:

$$i\frac{\partial A_{nm}(t)}{\partial t} = \Delta_{nm}^{(0)}A_{nm}(t) + \delta_{nm}^{(1)}B_{nm}(t) + \delta_{nm}^{(1)}C_{nm}(t) \tag{4}$$

$$i\frac{\partial B_{nm}(t)}{\partial t} = \delta_{nm}^{(1)}A_{nm}(t) + \Delta_{nm}^{(1)}B_{nm}(t) + \lambda_2 C_{nm}(t) + \delta_{nm}^{(2)}D_{nm}(t) \tag{5}$$

$$i\frac{\partial C_{nm}(t)}{\partial t} = \delta_{nm}^{(1)}A_{nm}(t) + \lambda_2 B_{nm}(t) + \Delta_{nm}^{(1)}C_{nm}(t) + \delta_{nm}^{(2)}D_{nm}(t) \tag{6}$$

$$i\frac{\partial D_{nm}(t)}{\partial t} = \delta_{nm}^{(2)}B_{nm}(t) + \delta_{nm}^{(2)}C_{nm}(t) + \Delta_{nm}^{(2)}D_{nm}(t) \tag{7}$$

where

$$\begin{aligned}
\Delta_{nm}^{(0)} &= \left(\omega_a - i\frac{\gamma}{2}\right)n + \left(\omega_b - i\frac{\gamma}{2}\right)m + \omega_q + \lambda_3 - i\gamma \\
\Delta_{nm}^{(1)} &= \left(\omega_a - i\frac{\gamma}{2}\right)(n+1) + \left(\omega_b - i\frac{\gamma}{2}\right)(m+1) - \lambda_3 - i\frac{\gamma}{2} \\
\Delta_{nm}^{(2)} &= \left(\omega_a - i\frac{\gamma}{2}\right)(n+2) + \left(\omega_b - i\frac{\gamma}{2}\right)(m+2) - \omega_q + \lambda_3 \\
\delta_{nm}^{(1)} &= \lambda_1\sqrt{(n+1)(m+1)},\ \ \delta_{nm}^{(2)} = \lambda_1\sqrt{(n+2)(m+2)}
\end{aligned} \tag{8}$$

Now, the solution of the system:

$$\begin{aligned}
A_{nm}(t) &= \sum_{j=1}^{4} z_{n,m} \mathrm{e}^{r_{nm}^{(j)}t} \eta_{nm}^{(j)} \\
B_{nm}(t) &= \sum_{j=1}^{4} z_{n,m} \mathrm{e}^{r_{nm}^{(j)}t} \zeta_{nm}^{(j)} = C_{nm}(t) \\
D_{nm}(t) &= \sum_{j=1}^{4} z_{n,m} \mathrm{e}^{r_{nm}^{(j)}t} \tau_{nm}^{(j)}
\end{aligned} \tag{9}$$

with

$$\eta_{nm}^{(j)} = -\frac{2\left(r_{nm}^{(j)}\delta_{nm}^{(1)}\delta_{nm}^{(2)} + i\delta_{nm}^{(1)}\Delta_{nm}^{(1)}\delta_{nm}^{(2)} - i\delta_{nm}^{(1)}\delta_{nm}^{(2)}\lambda_2\right)}{\prod_{k=1}^{4}\left(r_{nm}^{(j)} - r_{nm}^{(k)}\right)},\ \ k \neq j \tag{10}$$

$$\zeta_{nm}^{(j)} = \frac{-ir_{nm}^{(j)2}\delta_{nm}^{(2)} + r_{nm}^{(j)}\Delta_{nm}^{(0)}\delta_{nm}^{(2)} + r_{nm}^{(j)}\Delta_{nm}^{(1)}\delta_{nm}^{(2)} + i\Delta_{nm}^{(0)}\Delta_{nm}^{(1)}\delta_{nm}^{(2)} - r_{nm}^{(j)}\delta_{nm}^{(2)}\lambda_2 - i\Delta_{nm}^{(0)}\delta_{nm}^{(2)}\lambda_2}{\prod_{k=1}^{4}\left(r_{nm}^{(j)} - r_{nm}^{(k)}\right)},\ \ k \neq j \tag{11}$$

$$\tau_{nm}^{(j)} = \frac{r_{nm}^{(j)3} + ir_{nm}^{(j)2}\Delta_{nm}^{(0)} + 2r_{nm}^{(j)}\delta_{nm}^{(1)2} + 2ir_{nm}^{(j)2}\Delta_{nm}^{(1)} - 2r_{nm}^{(j)}\Delta_{nm}^{(0)}c - r_{nm}^{(j)}\Delta_{nm}^{(1)2} + r_{nm}^{(j)}\lambda_2^2 + \theta_{nm}}{\prod_{k=1}^{4}\left(r_{nm}^{(j)} - r_{nm}^{(k)}\right)},\ \ k \neq j \tag{12}$$

and

$$\begin{aligned}
\theta_{nm} &= 2i\delta_{nm}^{(1)2}\Delta_{nm}^{(1)} - i\Delta_{nm}^{(0)}\Delta_{nm}^{(1)2} + 2i\delta_{nm}^{(1)2}\lambda_2 + i\Delta_{nm}^{(0)}\lambda_2^2 \\
r_{nm}^{(1,2)} &= \mu^- \pm \nu^-,\ \ r_{nm}^{(3,4)} = \mu^+ \pm \nu^+,\ \ \mu^{\pm} = \frac{-x_1}{4} \pm \frac{y_1}{2},\ \ \nu^{\pm} = \frac{1}{2}\sqrt{y_2 \pm \frac{y_3}{4y_1}} \\
y_1 &= \sqrt{g_1 + \frac{g_2}{3g_3} + \frac{g_3}{3}},\ \ y_2 = 2g_1 - \frac{g_2}{3g_3} - \frac{g_3}{3},\ \ y_3 = 4x_1x_2 - x_1^3 - 8x_3 \\
g_1 &= \frac{x_1^2}{4} - \frac{2x_2}{3},\ \ g_2 = x_2^2 + 12x_4 - 3x_1x_3,\ \ g_3 = \sqrt[3]{\frac{d + \sqrt{d^2 - 4g_2^3}}{2}},\ \text{and} \\
d &= 2x_2^3 + 27(x_3^2 + x_1^2x_4) - 72x_2x_4 - 9x_1x_2x_3
\end{aligned} \tag{13}$$

Additionally:

$$x_1 = i\left(\Delta_{nm}^{(0)} + 2\Delta_{nm}^{(1)} + \Delta_{nm}^{(2)}\right)$$

$$x_2 = 2\delta_{nm}^{(1)2} - \Delta_{nm}^{(1)2} + 2\delta_{nm}^{(2)2} - 2\Delta_{nm}^{(1)}\Delta_{nm}^{(2)} - \Delta_{nm}^{(0)}\left(2\Delta_{nm}^{(1)} + \Delta_{nm}^{(2)}\right) + \lambda_2^2$$

$$x_3 = i\Big[-2\delta_{nm}^{(1)2}\Delta_{nm}^{(2)} + \Delta_{nm}^{(0)}\left(\Delta_{nm}^{(1)2} - 2\Delta_{nm}^{(2)2} + \Delta_{nm}^{(1)}\Delta_{nm}^{(2)} - \lambda_2^2\right) + \left(\Delta_{nm}^{(1)} - \lambda_2\right)\left(-2(\delta_{nm}^{(1)2} + \delta_{nm}^{(2)2}) + \Delta_{nm}^{(2)}(\Delta_{nm}^{(1)} + \lambda_2)\right)\Big] \text{ and} \quad (14)$$

$$x_4 = \left(\Delta_{nm}^{(1)} - \lambda_2\right)\left(-2\Delta_{nm}^{(0)}\delta_{nm}^{(2)2} - 2\delta_{nm}^{(1)2}\Delta_{nm}^{(2)} + \Delta_{nm}^{(0)}\Delta_{nm}^{(1)}\Delta_{nm}^{(2)} + \Delta_{nm}^{(0)}\Delta_{nm}^{(2)}\lambda_2\right)$$

Subsequent sections will explore the influence of various parameters on the correlation properties of a QB. These parameters include three coupling strengths, λ_1, λ_2, and λ_3, as well as decay parameters represented by κ_a, κ_b, and γ. The discussion will focus on key QB correlations, encompassing stored energy, power output, ergotropy, fluctuation levels, and quantum speed limit time. For consistency throughout the analysis, we will assume that the frequencies of the QB system are identical, expressed as $\omega_a = \omega_b = \omega_q = \omega_0$. The coherent state intensity for the two-mode are equal with $\alpha = \beta = 3$. All quantitative measures of the QB performance will be presented as functions of scaled time $\omega_0 t$, normalized by the system's characteristic frequency ω_0.

Stored energy

The evaluation of a QB's performance hinges critically on the quantification of its stored energy. Within the framework of Hamiltonian for the cells $\hat{H}_{QB}$, collective excitation states serve as the quantifiable measure of this energy. This energy embodies the system's capacity to perform work and is demonstrably influenced by various factors. These factors include the initial state of the QB $|\psi(0)\rangle$, the employed charging protocols, and the nature of its interactions with the surrounding environment. The energy stored $E(t)$ within the QB at time, t, can be calculated [24, 25]:

$$E(t) = \langle\psi(t)|\hat{H}_{QB}\langle\psi(t)| - \langle\psi(0)|\hat{H}_{QB}\langle\psi(0)| = \\ = \frac{\omega_q}{2}\sum_{n,m=0}^{\infty}\left(|A_{nm}(t)|^2 + |D_{nm}(t)|^2 - 2|B_{nm}(t)|^2 - 1\right) \quad (15)$$

where

$$\hat{H}_{QB} = \frac{\omega_q}{2}\sum_{i=1}^{2}\hat{\sigma}_z^i$$

Figure 1 investigates the impact of Hamiltonian coupling strengths and decay parameters on the stored energy, $E(t)$ in eq. (15), of the quantum battery. As illustrated in fig. 1(a), increasing the field-atom coupling strength λ_1 at constant dipole-dipole (λ_2) and ising (λ_3) couplings (both set to 0.1) leads to an enhancement of the average stored energy, $E(t)$. This behaviour exhibits characteristics of quasi-chaos. Conversely, for smaller values of λ_1, the stored energy exhibits periodic oscillations and approaches zero during certain time intervals. Figure 1(b) explores the effect of increasing the dipole-dipole coupling strength (λ_2) by varying its value (1, 2, and 5) while maintaining λ_1 and λ_3 at 0.1. At low values of λ_2, the stored energy exhibits slight oscillations over the measurement time. However, as λ_2 increases, the behaviour becomes more random, accompanied by a decrease in the maximum stored energy values. The influence of increasing the Ising coupling strength (λ_3) on the stored energy is depicted in fig. 1(c), where λ_3 is varied (1, 2, and 5) while λ_1 and λ_2 remain at 0.1.

Similar to the dipole-dipole coupling, increasing λ_3 leads to a decrease in the stored energy and an increase in fluctuations. Notably, the Ising coupling appears to have a more detrimental effect compared to the dipole-dipole coupling. This suggests that enhancing any coupling associated with the battery cells might reduce the stored energy and potentially distort the interaction between the cells and the charging source (photons). The impact of decoherence on the stored energy at constant couplings ($\lambda_1 = \lambda_2 = \lambda_3 = 0.1$) is presented in fig. 1(d). Here, increasing the decay parameters results in a decrease in the stored energy over time. This phenomenon is also observed in classical batteries. However, it is noteworthy that the decay of the atomic system exerts a weaker influence compared to the decay of the charging source.

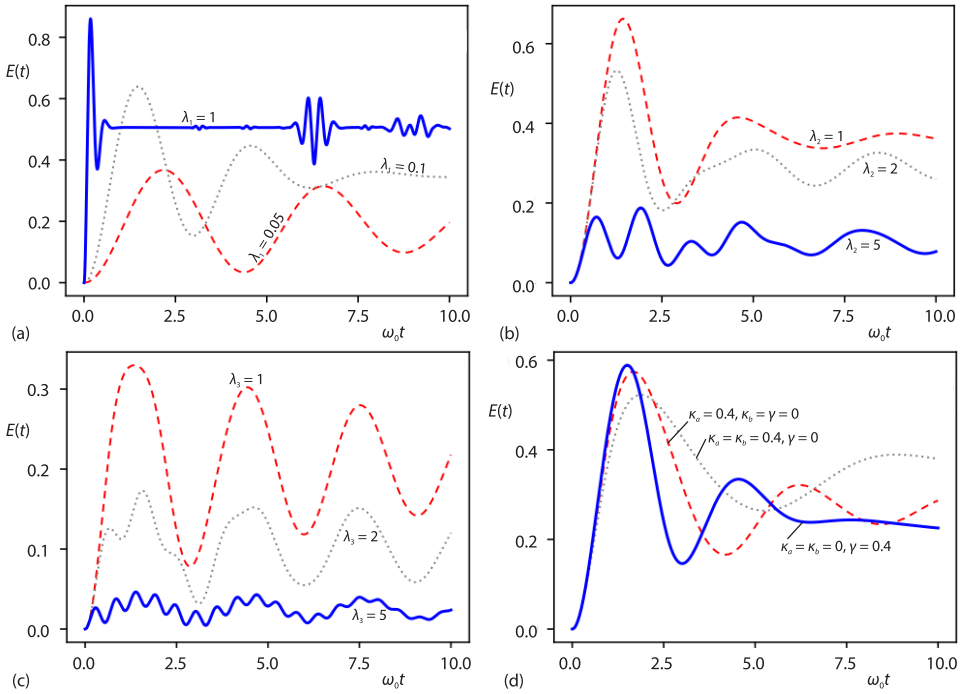

Figure 1. The energy against scaled time; (a) $\lambda_2 = \lambda_3 = 0.1$, $\kappa_a = \kappa_b = \gamma = 0$, but λ_1 changed, (b) $\lambda_1 = \lambda_3 = 0.1$, $\kappa_a = \kappa_b = \gamma = 0$, but λ_2 changed, (c) $\lambda_1 = \lambda_2 = 0.1$, $\kappa_a = \kappa_b = \gamma = 0$, but λ_3 changed, and (d) $\lambda_1 = \lambda_2 = \lambda_3 = 0.1$, but κ_a, κ_b and γ changed

Average charging power

In the context of evaluating results, the average charging power of a QB emerges as a paramount indicator of the system's temporal energy transfer rate [19]. This metric is demonstrably susceptible to the combined influence of charging efficiency and environmental factors, thereby significantly impacting the assessment of battery performance. A thorough understanding and subsequent optimization of average charging power are critical endeavors in maximizing the utility of quantum technologies. Efforts directed towards the refinement of charging mechanisms hold the potential to elevate both the efficiency and sustainability of quantum battery technologies [26], ultimately serving as a catalyst for innovation within quantum-enabled systems. The formal definition of average charging power is given [27]:

$$P_C(t) = \frac{E(t)}{t} \tag{16}$$

Figure 2 explores the impact of coupling strengths (λ_1, λ_2, λ_3) and decay parameters on the charging power of the QB. It is observed that the charging power tends towards a minimal value over time, regardless of whether the coupling strengths are increased or decreased. Figure 2(a) reveals several significant trends related to the field-atom coupling strength (λ_1) between the two-mode charger and the two quantum cells. Notably, the range of the average charging power exhibits a rapid increase for $\lambda_1 = 1$ compared to $\lambda_1 = 0.05$ and 0.1. This indicates that higher values of λ_1 significantly enhance the QB's charging power. Additionally, the duration of the charging process decreases as λ_1 increases. Moreover, fig. 2(b) presents notable trends concerning the dipole-dipole coupling strength (λ_2). The range of the average charging power exhibits a slight decrease for $\lambda_2 = 2$ and 5 compared to $\lambda_2 = 1$. This suggests that λ_1 values greater than zero lead to a marginal reduction in charging power, indicating a more moderated charging process. Furthermore, the charging duration remains stable across different λ_1 values, implying consistent charging behavior and contributing to a predictable and reliable charging cycle. Figure 2(c) investigates the effects of the Ising coupling strength (λ_3) on the average charging power. It is evident that the range of average charging power experiences a moderate decrease for $\lambda_3 = 2$ and 5 compared to $\lambda_3 = 1$. Higher Ising strength leads to a reduction in the charging power range, suggesting a more controlled charging process. Similar to the dipole-dipole coupling, the charging duration remains stable across different λ_3 values, indicating that λ_{13} does not significantly impact the charging time. However, chaotic behavior begins to emerge at $\lambda_3 = 5$, highlighting a potential increase in complexity at higher Ising interaction strengths. Overall, the average charging power behavior for λ_3 exhibits greater stability compared to λ_2 interaction but less stability than λ_1. The influence of decoherence parameters (κ_a, κ_b, and γ is

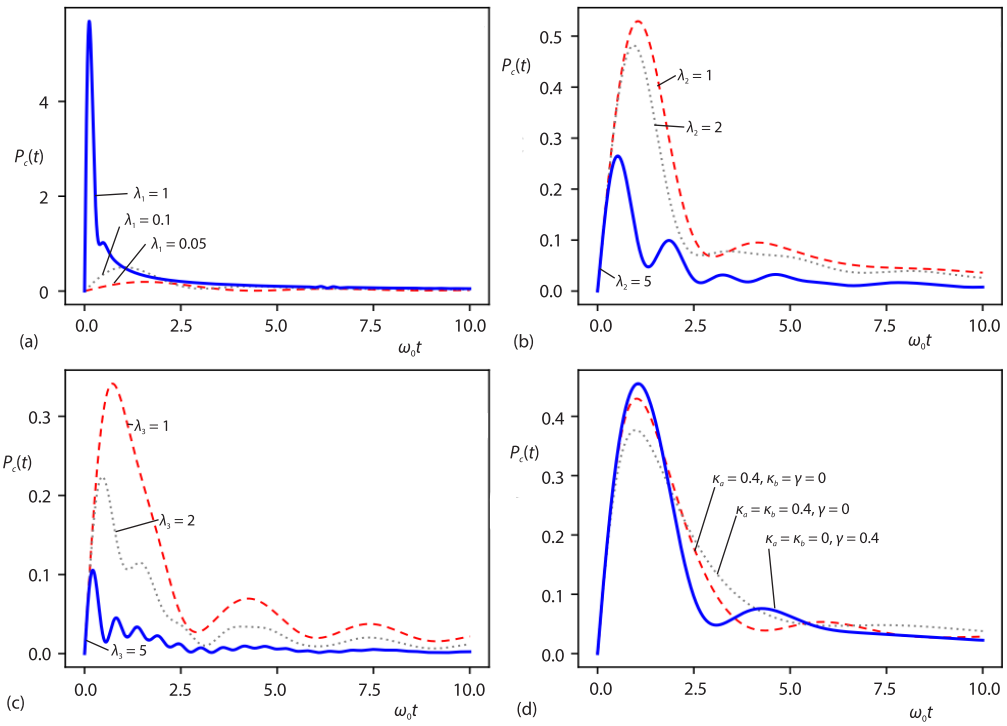

Figure 2. The average charging power against scaled time with the same parameters as that are displayed in fig. 1

examined in fig. 2(d). The range of average charging power exhibits a marginal decrease with increasing damping effects. This subtle reduction suggests that while damping has an impact, it does not drastically alter the charging power. The duration of the charging process remains stable across all cases, even with increasing numbers of damping parameters. This stability is observed for all two-mode charger parameters ($\kappa_a = 0.4$ and $\kappa_b = 0.4$) and the two quantum cells parameter ($\gamma = 0.4$). Despite the presence of damping, the charging period does not fluctuate significantly, ensuring a consistent charging cycle. The reduction in average charging power becomes slightly more apparent during the relaxation period until the completion of damping. This gradual decline highlights the persistent but manageable effect of environmental factors on the QB's performance. These observations align with our results in fig. 1(d), where various damping levels and their impact on the average charging power are detailed.

Ergotropy

Ergotropy, a critical measure for evaluating the effectiveness of a QB [28, 29], signifies the maximum amount of stored energy available for work extraction at a specific time during the QB's evolution (charging process). This quantity often deviates from the total stored energy due to locked energy within correlations, hindering its utilization for other purposes [14, 20]. To comprehensively derive this parameter, the QB's Hamiltonian is the fundamental building block. The density matrix, representing the statistical state of the QB at time, t, is obtained by applying the partial trace operation the atomic state of the system, expressed:

$$\hat{\rho}_{QB}(t) = Tr_f(|\psi(t))\langle\psi(t)|$$

The time-dependent density matrix of the QB can be given:

$$\begin{aligned}\hat{\rho}_{QB}(t) &\sum_{n,m=0}^{\infty}|A_{nm}(t)|^2|ee\rangle\langle ee| + \sum_{n,m=0}^{\infty}|B_{n+1,m+1}(t)|^2\left(|eg\rangle\langle eg| + |eg\rangle\langle ge| + |ge\rangle\langle ge|\right) + \\ &+ \sum_{n,m=0}^{\infty}|D_{n+2,m+2}(t)|^2|gg\rangle\langle gg| + \sum_{n,m=0}^{\infty}A_{nm}(t)D^*_{n+2,m+2}(t)|ee\rangle\langle gg| + \\ &+ \sum_{n,m=0}^{\infty}A_{nm}(t)B^*_{n+1,m+1}(t)\left(|ee\rangle\langle eg| + |ee\rangle\langle ge|\right) + \\ &+ \sum_{n,m=0}^{\infty}B_{n+1,m+1}(t)D^*_{n+2,m+2}(t)\left(|eg\rangle\langle gg| + |ge\rangle\langle gg|\right)(+h.c.\end{aligned} \tag{17}$$

where *h.r*. is the hermitian conjugate of the off-diagonal elements. The spectral decomposition [30] for the Hamiltonian, $\hat{H}_{QB}$:

$$\hat{H}_{QB} = \sum_{i=1}^{d} e_i|e_i\rangle\langle e_i| \tag{18}$$

where d is the number of levels in Hilbert space, and the eigenvalues are ordered such that $e_i < e_{i+1}$ associated to eigenstates $|e_i\rangle$, as well as the density matrix decomposition at time, t:

$$\hat{\rho}_{QB}(t) = \sum_{i=1}^{d} r_i(t)|r_i(t)\rangle\langle r_i(t)| \tag{19}$$

with respect to ordered eigenvalues such that $r_i(t) > r_{i+1}(t)$ with $|r_i(t)\rangle$ eigenstates. The eigen values of $\hat{\rho}_{QB}(t)$ are the roots of this equation $r_i^4 + l_1 r_i^3 + l_2 r_i^2 + l_3 r_i = 0$:

$$l_1 = -A - 2B - D,\ l_2 = -2|A|^2|B|^2 - |A|^2|D|^2 - 2|B|^2|D|^2 + 2(B)(D) + A(2B + D)$$
$$l_3 = 2\left[A|B|^2|D|^2 + B|A|^2|D|^2 + D|A|^2|B|^2 - |A|^2|B|^2|D|^2 - ABD\right]$$
$$\text{and } A = \sum_{nm=0}^{\infty} A_{nm}(t),\ B = \sum_{nm=0}^{\infty} B_{n+1,m+1}(t),\ D = \sum_{nm=0}^{\infty} D_{n+2,m+2}(t) \tag{20}$$
$$AB^* = \sum_{nm=0}^{\infty} A_{nm}(t)B^*_{n+1,m+1},\ AD^* = \sum_{nm=0}^{\infty} A_{nm}(t)D^*_{n+2,m+2}$$
$$BD^* = \sum_{nm=0}^{\infty} B_{n+1,m+1}(t)D^*_{n+2,m+2}$$

Now, the ergotropy [28, 31] is defined:

$$\epsilon(t) = Tr(\hat{\rho}_{QB}(t)\hat{H}_{QB}) - Tr(\hat{\eta}\hat{H}_{QB}) \tag{21}$$

$$\hat{\eta} = \sum_{i,j}^{d} r_j(t)e_i\left(\left|\left\langle r_j(t)\middle|e_i\right\rangle\right|^2 - \delta_{i,j}\right) \tag{22}$$

where

$$\hat{\eta} = \sum_{i=1}^{d} r_i(t)\left|e_i\right\rangle\left\langle e_i\right|$$

is the passive state (neither absorbed nor extracted) energy and $[\hat{\eta}, \hat{H}_{\mathrm{QB}}] = 0$ commutes with the Hamiltonian. Subsequently, the bound on the maximum and minimum extractable energy is given by $0 < \epsilon(t) < E(t)$.

Figure 3 explores the impact of various Hamiltonian parameters on the maximum extractable energy (ergotropy) of the QB. As shown in fig. 3(a), ergotropy increases with increasing values of λ_1. This suggests that stronger coupling between the field and the atoms enhances the amount of work extractable from the QB. However, this enhancement comes at a cost: As λ_1 increases from 0.05-0.1 and 1, the ergotropy behaviour exhibits progressively greater chaos and fluctuation. Figure 3(b) investigates the ergotropy of the QB, particularly the impact of varying the dipole-dipole interaction coupling (λ_2). While the range of ergotropy remains unstable across different λ_2 values, the average behaviour exhibits increasing chaos. Furthermore, the maximum values decrease as λ_2 changes from 1 to 2 and 5. This indicates that while the overall extractable work may be maintained, the system's stability deteriorates, leading to more erratic and unpredictable performance. The influence of varying Ising strengths along the z-axis (λ_3) between the two battery cells is depicted in fig. 3(c). The ergotropy range exhibits a decreasing trend as λ_3 varies from 1 -2 and 5, a more pronounced reduction compared to the x-axis interaction strength in fig. 3(b). Despite this decrease, the average number of fluctuations remains consistent. Interestingly, the system exhibits more chaotic behaviour compared to fig. 3(b), suggesting a degree of stabilization despite the decreasing ergotropy range. Figure 3(d) explores the impact of environmental parameters, specifically analyzing the decay of ergotropy as the number of effective parameters increases. Our findings reveal that as the number of parameters rises, the decay of ergotropy tends to increase. However, for specific parameter combinations (*e.g.*, κ_a= 0.4, κ_b = 0.4), the variability in behaviour is less pronounced. Additionally, for an average value of γ = 0.4, the decay occurs more rapidly compared to previous states, albeit with less chaotic behaviour. These observations highlight the intricate interplay between envi-

ronmental factors and the ergotropy of the QB system, underlining the importance of parameter optimization for enhancing energy extraction efficiency.

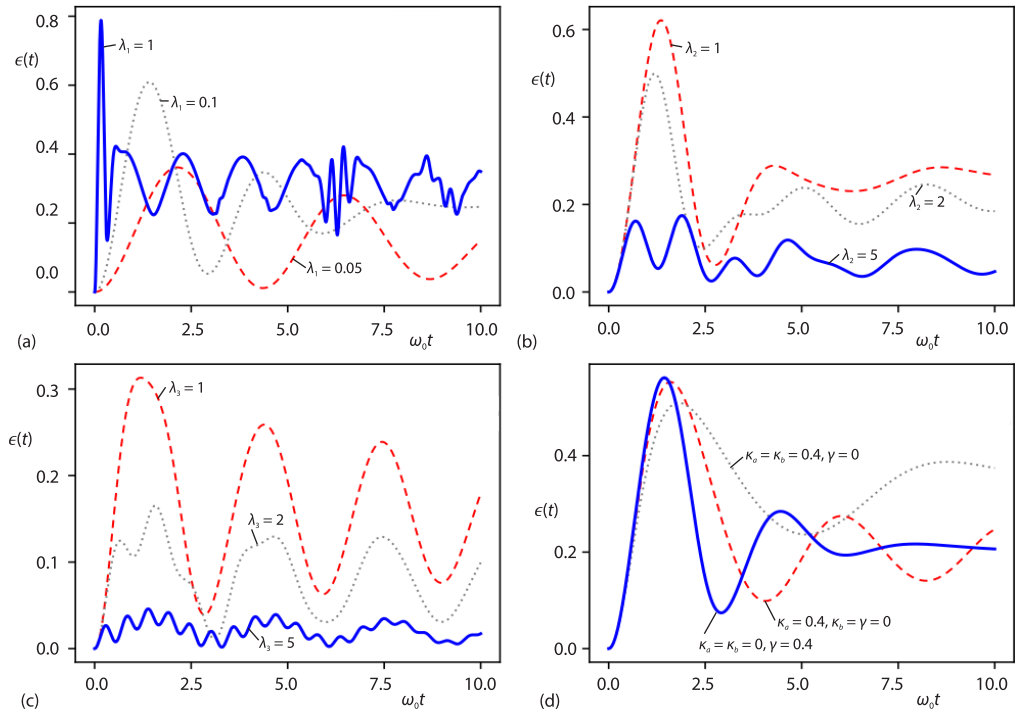

Figure 3. The ergotropy against scaled time with the same parameters as that are displayed in fig. 1

Energy fluctuation

Fluctuations of QB arise from the inherent discreteness of energy levels in quantum systems. This discreteness leads to intrinsic variability in energy storage capacities due to quantum mechanical phenomena. A thorough understanding and effective management of these fluctuations are crucial for enhancing both the performance and reliability of QB across various applications. In conjunction with traditional metrics like average energy and optimal charging duration [24], comprehending the temporal dynamics of stored energy becomes paramount. The energy fluctuations at defined time intervals is given [25, 32]:

$$\Sigma(t) = \sqrt{\langle\psi(0)|\delta\left(\hat{H}_{QB}\right)^2|\psi(0)\rangle - \left(\langle\psi(0)|\delta(\hat{H}_{QB}|\psi(0)\rangle\right)^2} \tag{23}$$

where

$$\delta(\hat{H}_{QB}) = \hat{H}(t)_{QB} - \hat{H}(0)_{QB}, \text{ and } \hat{H}(t)_{QB} = \hat{U}^{\dagger}\hat{H}_{QB}\hat{U}$$

the Hamiltonian evolved in time in the Heisenberg representation according to $\hat{H}$:

$$\hat{H}(t)_{QB} = e^{i\hat{H}t}\hat{H}_{QB}e^{-i\hat{H}t} = \hat{H}_{QB} + it[\hat{H}_{QB},\hat{H}] + \frac{(it)^2}{2!}[\hat{H},[\hat{H},\hat{H}_{QB}]] + \frac{(it)^3}{3!}[\hat{H},[\hat{H},[\hat{H},\hat{H}_{QB}]]] + \ldots.. \tag{24}$$

Figure 4 explores energy fluctuation as a measure of stability for our QB. The analysis of QB fluctuations in fig. 4(a) reveals the influence of varying coupling strengths (λ_1) between the charger and the cells. As λ_1 increases (0.05, 0.1, 1), the range of fluctuations also expands,

leading to progressively more erratic energy behaviour. For a low coupling strength ($\lambda_1 = 0.05$), the behaviour of fluctuations is minimal, indicating a regular energy transfer process. However, with increasing λ_1 (0.1 and 1) and time, fluctuations become more pronounced, suggesting a transitionwards more complex interactions. Notably, while the fluctuation range increase between $\lambda_1 = 0.1$ and 1 is modest, the system exhibits significantly greater chaos at $\lambda_1 = 1$. This highlights that strengthening the coupling beyond a moderate level enhances the system's chaotic nature without significantly expanding the fluctuation range. Figure 4(b) examines the influence of varying the interaction parameter (λ_2) between the two cells. As λ_2 takes on values of 1, 2, and 5, the range of energy fluctuations increases slightly, leading to moderately chaotic behaviour. The system's energy dynamics become progressively more erratic with increasing λ_2, but the fluctuation range differences between these values are relatively small compared to those observed for varying λ_1 in fig. 4(a). This suggests that while λ_2 affects stability, its impact is less pronounced than that of λ_1. The effects of varying the interaction parameter ($\lambda_3 = 1$, 2, and 5) between the two cells along the z-axis are shown in fig. 4(c). The function regularly osculate and relative chaotic behaviour as λ_3 increases. The fluctuation range aligns with the energy dynamics depicted in fig. 1(c), where the energy behaviour remains consistent despite variations in λ_3. These results suggest that λ_3 has a large influence in reducing the energy fluctuation compared to λ_3 and λ_2, contributing to a more predictable energy transfer process. Figure 4(d) explores the impact of environmental parameters on the system's stability, focusing on two-mode charger decay ($\kappa_a = \kappa_b = 0.4$) and quantum cell decay ($\gamma = 0.4$). The results indicate that energy fluctuations remain relatively stable in response to these decay effects. Notably, independent variations in the charger decay parameters (κ_a and κ_b) reveal significant differences in fluctuation behavior. However, the inclusion of the quantum cell decay parameter ($\gamma = 0.4$) shows only a slight change in the fluctuation range. Overall, this stability suggests that the sys-

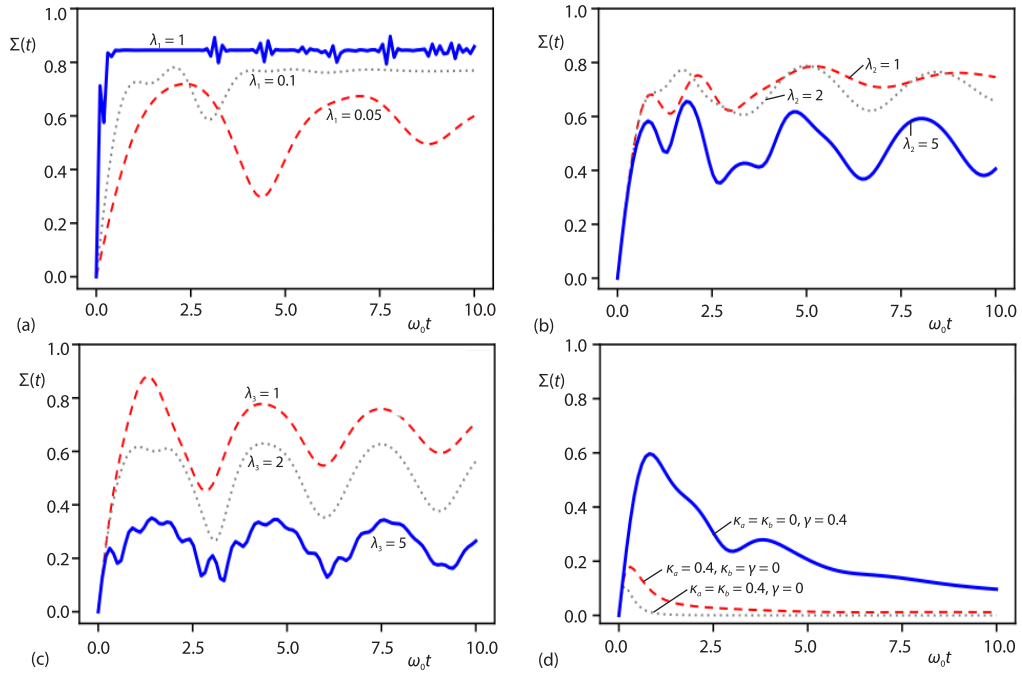

Figure 4. The energy fluctuation against scaled time with the same parameters as that are displayed in fig. 1.

tem exhibits resilience to moderate environmental decay effects, maintaining a consistent level of chaotic behavior.

Quantum speed limit

The concept of the quantum speed limit (QSL) imposes an inherent constraint on the rate at which a QB can be charged or discharged [33, 34]. This limitation arises from the fundamental principles of quantum mechanics, dictating the minimum time required for the system to transition between states. Unlike classical batteries, which could theoretically achieve instantaneous charging, QB necessitate a finite duration due to the complex interplay of energy levels within the system. Understanding this speed limit is crucial for refining charging protocols and optimizing the efficiency of these innovative energy storage devices. The formula of QSL is defined [35]:

$$\tau \geq \frac{\cos^{-1}\left[\left\langle \psi(0)|\psi(t)\right\rangle\right]}{\min\left[E(t), \sum(t)\right]} \tag{25}$$

Figure 5 illustrates the behavior of QSL for our quantum battery system. Notably, we initiate the time measurement at $t = 0.1$ since the QSL starts from infinity, indicating an inverse relationship with both quantum energy and quantum energy fluctuations, consistent with the definition provided in eq. (25). In fig. 5(a), we examine the QSL for varying values of the charger-battery cell interaction parameter, λ_1, specifically for 0.05, 0.1, and 1. It is evident that as the values of λ_1 decrease, the QSL increases significantly and exhibits chaotic behavior. This suggests a heightened sensitivity of the QSL to smaller λ_1 values, reflecting more erratic energy storage dynamics. Figure 5(b) presents the QSL behavior concerning λ_2, which represents the dipole interaction between the quantum cells. Here, the QSL shows minor differences in range and chaotic patterns for λ_2 values of 1, 2, and 5. This indicates that λ_2 has a less pronounced impact on the QSL compared to λ_1, though some degree of chaos is still observable. Similarly, fig. 5(c) explores the QSL for λ_3 values of 1, 2, and 5, revealing clearer differences compared

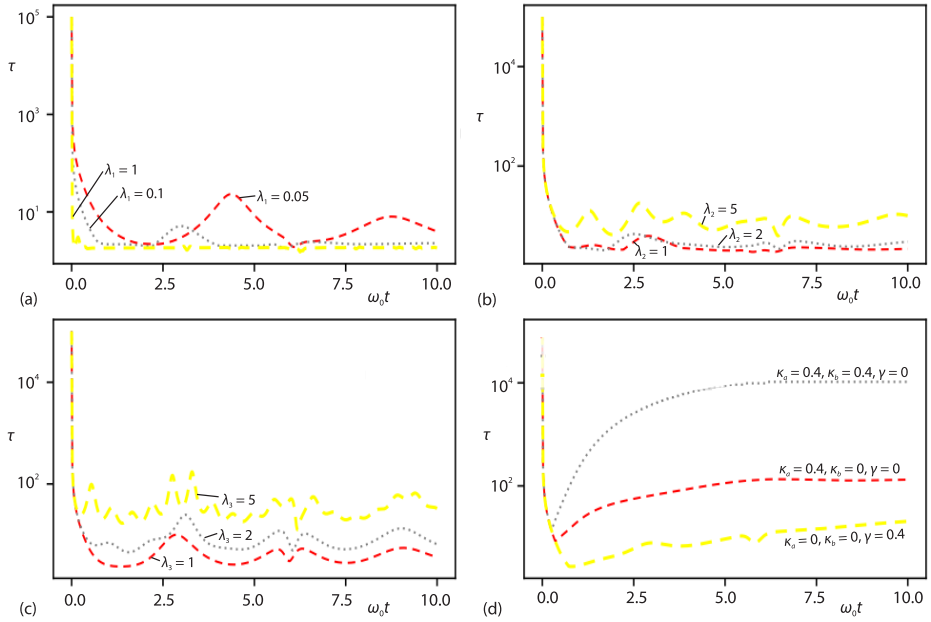

Figure 5. The QSL against scaled time with the same parameters as that are displayed in fig. 1

to λ_2 but still exhibiting chaotic behavior. This highlights the nuanced influence of λ_3 on the system's dynamics, suggesting a more complex interaction pattern affecting the QSL. Figure 5(d), we consider the effect of environmental noise on the QSL for different types of decay. As the system encounters increased environmental noise sources for both the charger modes and quantum cells, the QSL escalates dramatically and increase. However, the increasing rate in the presence of charger modes greater than when we take the noisy of quantum cell into account. This observation supports the inverse proportional relationship between energy storage, energy fluctuation, and the QSL. The increased noise induces greater fluctuations in the energy states, thereby elongating the time required to achieve optimal energy storage.

Conclusion

This study conducted a comprehensive investigation of quantum battery systems, focusing on the interplay between two-mode field charging, qubit interactions, and environmental effects. An analytical solution of the system enabled the examination of energy behavior in relation various parameters, including coupling strengths (charger-cell, dipole, Ising), and environmental decay rates. The analysis further explored stored energy, average charging power, ergotropy, energy fluctuations, and the QSL for these same parameter values. Our key findings reveal that charger-cell coupling exerts a significant influence on the stability and efficiency of the charging process. While higher coupling values lead to more chaotic energy behavior, they also facilitate smoother operation at optimal levels. The effects of dipole and Ising interactions between the cells themselves were more subtle but crucial for preventing instability and dissipating energy transfer inefficiencies. Environmental parameters were found to play a critical role, with increased decay leading to more stable and predictable QSL, ultimately improving overall battery performance. Investigations into average charging power and kinetic entropy revealed how different parameter settings could optimize energy storage and retrieval, enhancing the practical utility of QB. The study of energy fluctuations provided insights into the inherent stability of the system, while QSL analysis emphasized the importance of fast and efficient energy transitions. Variations in parameters led to significant changes in QSL, with increased environmental noise causing larger fluctuations and longer charging times. This finding highlights the inherent trade-off between QSL, energy storage capacity, and energy fluctuations, emphasizing the importance of balancing these factors for optimal performance. By exploring various scenarios and parameter configurations, we identified strategies to improve the performance of QB, making them more efficient and reliable. These findings offer valuable insights into the field of quantum energy storage and illuminate potential avenues for future research. The comprehensive nature of this study contributes significantly to the scientific understanding of QB, providing a detailed roadmap for enhancing the efficiency and stability of quantum energy storage systems.

Acknowledgment

The authors extend their appreciation to Taif University, Saudi Arabia, for supporting this work through project number (TU-DSPP-2024-71).

References

[1] Weber, A. Z., *et al.*, Redox Flow Batteries: A Review, *J. Appl. Electrochemistry*, *41* (2011), Sept., pp. 1137-1164
[2] Pan, F., Wang, Q., Redox Species of Redox Flow Batteries: A Review, *Molecules*, *20* (2015), 11, pp. 20499-20517
[3] Schmidt-Rohr, K., How Batteries Store and Release Energy: Explaining Basic Electrochemistry, *J. Chem. Educ.*, *95* (2018), 10, pp. 1801-1810
[4] Geppert, L., Quantum Transistors: Toward Nanoelectronics, *IEEE Spectrum*, *37* (2000), 9. pp. 46-51
[5] Hedges, M. P., *et al.*, Efficient Quantum Memory for Light, *Nature*, *465* (2010), 7301, pp. 1052-1056

[6] Ladd, T. D., *et al*., Quantum Computers, *Nature*, *464* (2010), 7285, pp. 45-53
[7] Shen, H., *et al*., Quantum Optical Diode with Semiconductor Microcavities, *Phys. Rev. A*, *90* (2014), 2, 023849
[8] McRae, A., *et al*., Graphene Quantum Strain Transistors, *Phys. Rev. Appl. 11* (2019), 5, 054019
[9] Alicki, R., Fannes, M., Entanglement Boost For Extractable Work from Ensembles of Quantum Batteries, *Phys. Rev. E*, *87* (2013), 4, 042123
[10] Andolina, G. M., *et al*., Quantum *vs*. Classical Many-Body Batteries, *Phys. Rev. B*, *99* (2019), 20, 205437
[11] Kamin, F., *et al.*, Non-Markovian Effects on Charging and Self-Discharging Process of Quantum Batteries, *New J. Phy*., *22* (2020), 8, 083007
[12] Santos, A. C., Quantum Advantage of Two-Level Batteries in the Self-Discharging Process, *Phys. Rev. E*, *103* (2021), 4, 042118
[13] Farina, D., *et al*., Charger-Mediated Energy Transfer for Quantum Batteries: An Open-System Approach, *Phys. Rev. B*, *99* (2019), 3, 035421
[14] Andolina, G. M., *et al.*, Extractable Work, the Role of Correlations, and Asymptotic Freedom in Quantum Batteries, *Phys. Rev. Lett*., *122* (2019), 4, 047702
[15] Chang, W., *et al.*, Optimal Building Block of Multipartite Quantum Battery in the Driven-Dissipative Charging, *New J. Phy*., *23* (2021), 10, 103026
[16] Le, T. P., *et al*., Spin-Chain Model of A Many-Body Quantum Battery, *Phys. Rev. A*, *97* (2018), 2, 022106
[17] Ghosh, S., et al., Fast Charging of a Quantum Battery Assisted by Noise, *Phys. Rev. A*, *104* (2021), 3, 032207
[18] Hovhannisyan, K. V., *et al*., Entanglement Generation is Not Necessary for Optimal Work Extraction, *Phys. Rev. Lett*., *111* (2013), 24, 240401
[19] Binder, F. C., *et al*., Quantacell: Powerful Charging of Quantum Batteries, *New J. Phy.*, *17* (2015), 7, 075015
[20] Ghosh, S., *et al*., Enhancement in the Performance of a Quantum Battery by Ordered and Disordered Interactions, *Phys. Rev. A*, *101* (2020), 3, 032115
[21] Rossini, D., *et al.*, Many-Body Localized Quantum Batteries, *Phys. Rev. B*, (2019), 11, 115142
[22] Kamin, F., *et al*., Entanglement, Coherence, and Charging Process of Quantum Batteries, *Phys. Rev. E*, *102*, (2020), 5, 052109
[23] Araya-Sossa, K., Mundarain, D., Geometrical Correlations as a Resource for Non-Local Extractable Work, *Ann. Phys*., *404* (2019), Mar., pp. 81-92
[24] Campaioli, F., *et al*., Enhancing the Charging Power of Quantum Batteries, *Phys. Rev. Lett.*, *118* (2017), 150601
[25] Crescente, A., *et al.*, Ultrafast Charging in a Two-Photon Dicke Quantum Battery, *Phys. Rev. B*, *102* (2020), 24, 245407
[26] Quach, J. Q., *et al*., Superabsorption in an Organic Microcavity: Toward a Quantum Battery. *Sci. Adv.*, *8* (2022), 2, 3160
[27] Julia-Farre, S., *et al*., Bounds on the Capacity and Power of Quantum Batteries. *Phys. Rev. Res.*, *2* (2020), 2, 023113
[28] Francica, G., *et al*., Quantum Coherence and Ergotropy, *Phys. Rev. Lett*., *125* (2020), 18,180603
[29] Cakmak, B., Ergotropy from Coherences in an Open Quantum System, *Phys. Rev. E*, *102* (2020), 042111
[30] Antoniou, I., Tasaki, S., Generalized Spectral Decompositions of Mixing Dynamical Systems, *Int. J. Quantum Chem*., *46* (1993), 3, pp. 425-474
[31] Koshihara, K., Yuasa, K., Quantum Ergotropy and Quantum Feedback Control, *Phys. Rev. E*, *107* (2023), 064109
[32] Wang, W., *et al.*, Application of Energy Storage in Integrated Energy Systems – A Solution Fluctuation and Uncertainty of Renewable Energy, *J. Energy Storage*, *52* (2022), 104812
[33] Deffner, S., Campbell, S., Quantum Speed Limits: from Heisenberg's Uncertainty Principle to Optimal Quantum Control., *J. Phys. A: Math. Theor.*, *50* (2017), 45, 453001
[34] del Campo, A., *et al*., Quantum Speed Limits in Open System Dynamics, *Phys. Rev. Lett*., *110* (2013), 5, 050403
[35] Campaioli, F., *et al*., Colloquium: Quantum Batteries, *Rev. Mod. Phys*., *96* (2024), 3, 031001

Paper submitted: June 11, 2024
Paper revised: September 23, 2024
Paper accepted: October 2, 2024